

Cyclotron absorption in rotating pulsar magnetospheres

D. Fussell, Q. Luo^{*} and D. B. Melrose

Research Centre for Theoretical Astrophysics, School of Physics, University of Sydney, NSW 2006, Australia

Accepted 2003 May 1. Received 2003 February 21

ABSTRACT

Cyclotron absorption in relativistic pulsar plasma is discussed in detail. The effect of cyclotron absorption on pulsar radio emission is examined, including the corotation of the plasma with the pulsar. The absorption coefficients for the two escaping modes, the X and LO modes, are derived and used to evaluate numerically the absorption profile across the emission beam. As a result of the rotation, the absorption is generally not axially symmetric across the beam, which can lead to potentially observable features of the pulse profile.

Key words: plasmas – polarization – radiation mechanisms: non-thermal – pulsars: general.

1 INTRODUCTION

Observational evidence (Blaskiewicz, Cordes & Wasserman 1991) suggests that pulsar radio emission is produced in the inner magnetosphere, where the (Doppler-shifted) cyclotron frequencies of electrons (including positrons) is much higher than the wave frequency. Along the ray path of the escaping emission, the cyclotron frequency decreases, and cyclotron absorption becomes relevant where the cyclotron frequency is equal to the wave frequency (e.g. Blandford & Scharlemann 1976; Mikhailovskii et al. 1982; Lyubarskii & Petrova 1998). Luo & Melrose (2001, hereafter LM) included intrinsically relativistic effects on the wave properties in the pulsar plasma in treating cyclotron absorption, and pointed out that an asymmetry in the observed pulse profile can arise due to the combined effects of rotation and cyclotron absorption. In this paper we explore this effect by developing a model that includes propagation of the escaping rays and rotation of the plasma, as well as the cyclotron absorption itself.

We assume a conventional polar-cap model (Sturrock 1971; Ruderman & Sutherland 1975; Arons 1983). Primary particles, with number density close to the Goldreich–Julian value, are accelerated to extremely high energies ($\gamma_p \sim 10^6$) by a field-aligned electric field. These primaries emit high-energy photons, and these photons create secondary pairs in an electromagnetic cascade (e.g. Daugherty & Harding 1982) concentrated in a pair-formation front (PFF). The secondary pairs constitute the bulk of the magnetospheric plasma in the polar-cap regions, and this plasma flows outwards, becoming the pulsar wind beyond the light cylinder (LC). Earlier models for the cascade (Daugherty & Harding 1982) show that it produces extremely relativistic plasma, with a highly relativistic spread in particle energies in the rest frame of the plasma. More recent models (Zhang & Harding 2000; Hibschan & Arons 2001) support this general conclusion, but favour a lower multiplicity, $M \sim 100$, which is the ratio of secondaries to primaries, and lower energies (Lorentz factors $\gamma \sim 100$) for the secondaries than in the

earlier models. In the strong magnetic field, typically $B \sim 10^8$ T at the stellar surface, the secondaries are created either in their ground Landau state, if the field is sufficiently strong (Weise & Melrose 2001), or in higher Landau states and rapidly radiate away their perpendicular energies to relax to their lowest Landau state. As a consequence, the momentum distribution of pulsar plasma well inside the LC is one-dimensional. The radio emission is thought to be produced in this one-dimensional, highly relativistic pair plasma at a height well above the PFF but well inside the LC. We are concerned with refraction and cyclotron absorption in the corotating pulsar plasma between the point of emission and the LC.

As in earlier investigations of the effect of cyclotron absorption on a beam of escaping pulsar radio emission (Blandford & Scharlemann 1976; Mikhailovskii et al. 1982), we assume a dipole magnetic field, which falls rapidly with radial distance from the star, $B \propto R^{-3}$. In the region where cyclotron absorption occurs, an electron that absorbs a cyclotron photon is excited from its ground Landau state to its first Landau state. Subsequently the electron re-emits a cyclotron photon, relaxing back to its ground state; the re-emitted photons have a wide angular distribution and are probably not observable. With the cyclotron absorption treated in a cold pulsar plasma (Blandford & Scharlemann 1976; Mikhailovskii et al. 1982; Lyubarskii & Petrova 1998), it was found that the radio emission should be heavily absorbed, which is difficult to reconcile with observations. LM treated cyclotron absorption in an intrinsically relativistic pulsar plasma and found that it should occur within the LC for a wide class of pulsars, including millisecond pulsars, and that marginal absorption in a preferred subpopulation of pulsars should cause them to exhibit an observational signature of preferential damping of the trailing component in conal pulse profiles. This effect of cyclotron absorption is explored in detail here.

In this paper, we include relativistic effects on the dispersion in the plasma, which is birefringent with two natural wave modes, referred to here as the X and LO modes. For simplicity we ignore gyrotronic effects, so that the waves are linearly polarized. The neglect of gyrotronic effects precludes any systematic discussion of circular polarization. To relax this assumption, so that the natural modes are

^{*}E-mail: q.luo@physics.usyd.edu.au

elliptically polarized in general, one needs to take into account the ellipticity both at the point of emission and in the region of cyclotron absorption, as well as distinguishing between the opposing effects of absorption by electrons and positrons on the handedness of the radiation. With gyrotropy neglected, the net effect of absorption by electrons and positrons has no preferred handedness.

In Section 2, the cyclotron resonance condition is discussed and the absorption coefficient is evaluated numerically using the formalism for the plasma response adopted by Kennett, Melrose & Luo (2000). Numerical calculation of absorption across the emission beam is described in Section 3, and the implications of these profiles for observations are discussed in Section 4.

2 CYCLOTRON ABSORPTION IN PULSAR PLASMAS

The cyclotron resonance condition of relevance here is

$$\omega - k_{\parallel} v_{\parallel} \pm \Omega_e / \gamma = 0, \quad (1)$$

where $\Omega_e = eB/m$ is the cyclotron frequency, k_{\parallel} is the parallel (to the local magnetic field, \mathbf{B}) wavevector, v_{\parallel} is the particle velocity (we set $c = 1$) and $\gamma = (1 - v_{\parallel}^2)^{-1/2}$. The ‘+’ and ‘-’ signs correspond respectively to the anomalous cyclotron resonance (ACR) and the normal cyclotron resonance (NCR). Only NCR corresponds to cyclotron absorption in the conventional sense. In ACR the electron jumps from its ground Landau state to its first excited state through stimulated emission of a photon, and this is possible, *inter alia*, only for waves with refractive index greater than unity. Although ACR is not discussed in detail here, for formal purposes it is convenient to treat the two processes together.

On multiplying the two equations (1) by each other to eliminate the \pm signs, one obtains a quadratic equation for v_{\parallel} in terms of the phase speed $v_{\phi} = \omega/k_{\parallel}$ parallel to \mathbf{B} . The solutions are ellipses, and examples are plotted in Fig. 1, where the NCR and ACR are distinguished by solid and dashed lines, respectively. The boundary separating the NCR and ACR regimes is $v_{\phi} = v_{\parallel} = \pm 1$. It can be seen that for a forward propagating wave ($k_{\parallel} > 0$ or $v_{\phi} > 0$) the parameter space for the NCR is considerably broader than that for the ACR. For algebraic purposes it is convenient to write the solutions of the quadratic equation as

$$v_{r\pm} = \left[\omega k_{\parallel} \pm \Omega_e (k_{\parallel}^2 + \Omega_e^2 - \omega^2)^{1/2} \right] / (k_{\parallel}^2 + \Omega_e^2),$$

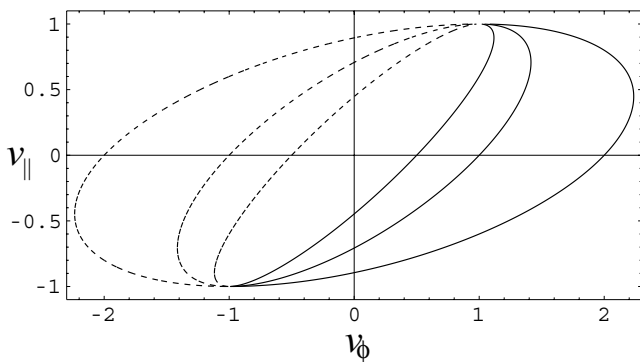


Figure 1. The cyclotron resonance condition. The resonance velocities are shown as ellipses in $v_{\parallel} - v_{\phi} = \omega/k_{\parallel}$ space: $\Omega_e/k_{\parallel} = 0.5$ (inner ellipse), 1 (intermediate ellipse), and 2 (outer ellipse). The solid and dashed curves correspond respectively to NCR and ACR. The boundary between the NCR and ACR regimes is $v_{\phi} = v_{\parallel}$.

which are interpreted as the resonance velocities. Note that the \pm signs in these solutions are unrelated to the \pm signs in equation (1): one has $v_{\parallel} = v_{r+}$ above the extrema along the v_{ϕ} axis for the curves in (1), and $v_{\parallel} = v_{r-}$ below these extrema.

2.1 General formalism for absorption coefficient

Wave damping is treated here using the formalism discussed by Melrose & McPhedron (1991). Specifically, the wave properties are determined by the dielectric tensor, K_{ij} , which can be separated into Hermitian and anti-Hermitian parts, K_{ij}^H and K_{ij}^A , describing respectively reactive (wave modes) and dissipative (such as instability and absorption) components. The absorption coefficient for a particular wave mode, M , is obtained from K_{ij}^A as (Melrose & McPhedron 1991)

$$\Gamma_M = -2(\omega_l - \mathbf{k}_l \cdot \mathbf{v}_g) = -2i\omega R_E K^A, \quad K^A = e_i^* K_{ij}^A e_j, \quad (2)$$

where \mathbf{e} is the polarization vector, R_E is the fraction of total wave energy in the electric field and \mathbf{v}_g is the wave group velocity. Both the frequency and wavevector may have imaginary components, ω_l and \mathbf{k}_l , corresponding respectively to temporal and spatial damping. The ratio R_E can be written in the form

$$R_E = \frac{\omega}{[\partial(\omega^2 K)/\partial\omega]}, \quad K = e_i^* K_{ij} e_j, \quad (3)$$

where $\omega = \omega_M(\mathbf{k})$ is the dispersion relation for the wave mode M .

In writing down the dielectric tensor, K_{ij} , we assume the non-gyrotropic limit, where the distributions of electrons and positrons are identical. The anti-Hermitian part of the dielectric tensor, K_{ij}^A , is determined using the Landau prescription (cf. Appendix A). Waves are considered in the plasma rest frame with the 3-axis along \mathbf{B} and \mathbf{k} in the (1, 3)-plane at a propagation angle θ to \mathbf{B} . The non-zero components of K_{ij}^A are

$$\begin{aligned} K_{11}^A = K_{22}^A &= i\pi \frac{\omega_p^2 \Omega_e}{2\omega^2} \left[\sum_{\pm} \frac{\gamma_{\pm} F(u_{\pm})}{|k_{\parallel} - u_{\pm} \Omega_e|} H(v_{\phi} - v_{r\pm}) \right. \\ &\quad \left. - \frac{\gamma_{+} F(u_{+})}{|k_{\parallel} + u_{+} \Omega_e|} H(v_{r+} - v_{\phi}) \right], \\ K_{13}^A = K_{31}^A &= i\pi \frac{\omega_p^2 \tan \theta}{2\omega v_{\phi}} \left[\sum_{\pm} \frac{\gamma_{\pm} u_{\pm} F(u_{\pm})}{|k_{\parallel} - u_{\pm} \Omega_e|} H(v_{\phi} - v_{r\pm}) \right. \\ &\quad \left. + \frac{\gamma_{+} u_{+} F(u_{+})}{|k_{\parallel} + u_{+} \Omega_e|} H(v_{r+} - v_{\phi}) \right], \\ K_{33}^A &= i\pi \frac{\omega_p^2 \tan^2 \theta}{2v_{\phi}^2 \Omega_e} \left[\sum_{\pm} \frac{\gamma_{\pm} u_{\pm}^2 F(u_{\pm})}{|k_{\parallel} - u_{\pm} \Omega_e|} H(v_{\phi} - v_{r\pm}) \right. \\ &\quad \left. - \frac{\gamma_{+} u_{+}^2 F(u_{+})}{|k_{\parallel} + u_{+} \Omega_e|} H(v_{r+} - v_{\phi}) \right] \\ &\quad - i\pi \frac{\omega_p^2 v_{\phi}}{\omega} \frac{\partial F(\gamma v_{\parallel})}{\partial v_{\parallel}} \Big|_{v_{\parallel}=v_{\phi}}, \end{aligned} \quad (4)$$

where $v_{r\pm}$ are the resonance velocities, ω_p is the plasma frequency, $F(u)$ is the normalized (one-dimensional) particle distribution function with $u = \gamma v_{\parallel}$, $H(x)$ is the Heaviside function with $H(x) = 0$ for $x < 0$ and $H(x) = 1$ otherwise, $u_{\pm} = \gamma_{\pm} v_{r\pm}$, and $\gamma_{\pm} = (1 - v_{r\pm}^2)^{-1/2}$. The derivation of (4) involves integrands with δ -functions that are

not defined for $v_\phi^2 = 1 + (\Omega_e/k_\parallel)^2$, requiring $v_\phi^2 < 1 + (\Omega_e/k_\parallel)^2$. The terms involving the sums over \pm in each component of (4) are for cyclotron absorption due to NCR. The terms involving $H(v_\phi - v_{r\pm})$ are associated with cyclotron instability due to ACR (e.g. Kazebegi, Machabeli & Melikidze 1991). The last term in K_{33}^A is for Landau damping, which occurs (like ACR) only for subluminal waves, and only for waves with a parallel (relative to \mathbf{B}) component to their polarization. Landau absorption is important for the Alfvén mode (e.g. Arons & Barnard 1986), and negative Landau absorption of LO-mode waves is one of the conventional emission mechanisms. Only cyclotron absorption due to NCR is discussed in this paper.

2.2 The X and LO modes

The absorption coefficient is examined first in the plasma frame for the two modes that escape the magnetosphere, the X and LO modes. The polarization vector is $\mathbf{e} = (0, i, 0)$ for the X mode and of the form $\mathbf{e} = (e_1, 0, e_3)$ for the LO mode (cf. Melrose et al. 1999 for the details). The effect of the cyclotron resonance on the dispersion in a relativistic pulsar plasma was treated recently by Kennett et al. (2000). For low frequency, and oblique ($\theta \geq 0$) propagation, the waves are superluminal ($v_\phi > 1$), and the O mode has both longitudinal and transverse polarization components. (The X mode is strictly transverse when gyrotopry is neglected.) These properties apply in the frequency range between the cut-off frequency, $\omega_c \approx \omega_p/\langle\gamma\rangle^{1/2}$, and the crossover frequency, $\omega_{co} \approx \omega_p\langle\gamma\rangle^{1/2}$, where $\langle\gamma\rangle$ is the average Lorentz factor. For high frequencies, the O mode becomes nearly transverse and both modes have refractive index $n = k/\omega \approx 1$. Gradients in plasma parameters cause refraction, especially for low frequencies, $\omega \sim \omega_c$, which affects the LO mode more than the X mode, which has $n \rightarrow 1$ for $B \rightarrow \infty$ (Barnard & Arons 1986).

2.3 Numerical evaluation of Γ_M

To calculate the absorption coefficient, one needs a specific form of plasma distribution, $F(u)$. Although the form of $F(u)$ is not well constrained (Daugherty & Harding 1982; Shibata, Miyazaki & Takahara 1998), a thermal (Jüttner) distribution in the rest frame is favoured in one recent calculation of pair creation (Arendt & Eilek 2002). Convenient choices are either the Jüttner distribution (e.g. Gedalin, Melrose & Gruman 1998; Asseo & Khechinashvili 2002) or bell-type distributions (Gedalin et al. 1998), given by

$$F(u) \propto e^{-\rho\gamma} \quad (\text{Jüttner}), \quad (5)$$

$$F_n(u) \propto (u^2 - u_m^2)^n H(u_m^2 - u^2), \quad (\text{bell type}), \quad (6)$$

where ρ is the inverse temperature, in terms of the electron rest energy, and u_m is a maximum four velocity. The parameter n labels different distributions, with $n = 0$ called the water bag distribution and $n = 2$ the soft bell distribution.

An example of Γ_X evaluated using these distributions is shown in Fig. 2. Dispersion is insensitive to the particular choice of distribution (e.g. Melrose et al. 1999) and this also applies reasonably to the basic shape of the absorption coefficient (e.g. as a function of wave frequency). As shown in Fig. 2, different forms of distribution function imply slightly different absorption as a function of frequency for given plasma parameters. However, the important features are robust, and, given the large uncertainty in plasma parameters, the difference between distribution functions is minor. In the following discussion, we assume the soft bell distribution, which allows all important wave properties to be determined with relative ease of calculations (Kennett et al. 2000).

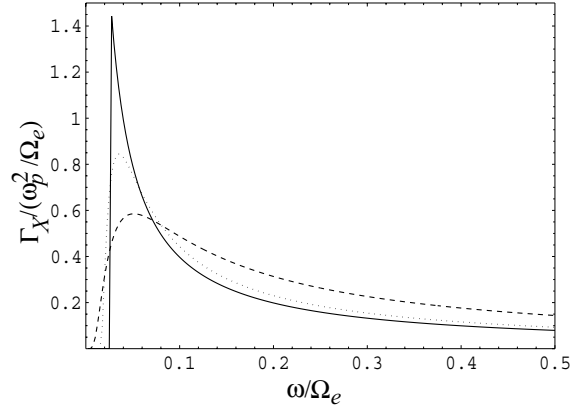


Figure 2. The cyclotron absorption coefficient, Γ_X , in the plasma frame at $\theta = 0$ for the Jüttner (dotted), water bag (solid) and soft bell (dashed) distributions. The plasma parameters are $\langle\gamma\rangle = 10$ and $\omega_p/\Omega_e = 10^{-3}$.

The absorption coefficient is shown in Fig. 3 for both modes for soft bell distributions in the plasma frame. The absorption coefficient peaks near the relativistic cyclotron frequency $\omega \sim \Omega_e/\langle\gamma\rangle$ and, for the most part, it is independent of θ . The absorption peak is normalized to $\Gamma_M \approx 0.8(\omega_p^2/\Omega_e)$ ($M = X, LO$) and the peak value of the ratio $\Gamma_M/(\omega_p^2/\Omega_e)$ is an insensitive function of $\langle\gamma\rangle \gg 1$ and of $\omega \ll \Omega_e$.

The cyclotron resonance is encountered at high frequencies where both modes are essentially transverse, and the difference between Γ_X and Γ_{LO} is small. A possible exception is the longitudinally polarized LO mode near the resonance, which occurs for $\theta \approx 0$ and $\omega \sim \omega_c$. For $\omega \sim \Omega_e/\langle\gamma\rangle$, this regime corresponds to $\theta \leq \omega_p^2\langle\gamma\rangle/\Omega_e^2$, requiring the Alfvén speed $v_a = \Omega_e/\omega_p\langle\gamma\rangle^{1/2} \sim 1$, which is implausible in the cyclotron resonance region for most pulsars.

Qualitative features of the cyclotron absorption coefficient can be summarized as follows. The absorption increases sharply with increasing ω from below its peak and falls as $\sim\omega^{-1}$ thereafter. The absorption coefficients vary only slightly from small ($\theta < 1$) to large ($\theta > 1$) propagation angles. For $\theta < 1$, where the limit $v_\phi \geq 1$ and $v_\phi \ll \Omega_e/k_\parallel$ applies, absorption is due mainly to the resonant particles with velocity $v_{r-} \sim -1$ in the wing of the particle distribution function. In the rest frame of the plasma, the absorption coefficient, Γ_M , is the same for both backward- and forward-propagating waves, as a result of our assumption that in the rest frame the distributions of electrons and positrons are symmetric under $v_\parallel \rightarrow -v_\parallel$.

2.4 Absorption coefficient in the pulsar frame

In the plasma frame, Γ_X can be written in the form

$$\begin{aligned} \Gamma_X(\omega; \theta) &\approx \frac{\pi}{2} \frac{\omega_p^2}{\omega} F(\gamma_\pm v_{r\pm}) \\ &\approx \frac{\omega_p^2}{\Omega_e} 0.4 \quad \text{for} \quad \frac{\omega}{\Omega_e} \sim \frac{1}{\langle\gamma\rangle}, \end{aligned} \quad (7)$$

with $(\pi/2)\langle\gamma\rangle F(\gamma_\pm v_{r\pm}) \approx 0.4$ for $|u_m| \gg 1$. One can obtain Γ_X in the pulsar frame by transforming the individual components on the right-hand side of (7) or using the usual Lorentz transform of damping rates as

$$\Gamma_X(\omega; \theta) = \gamma_s \left(1 - \frac{v_s}{v_\phi}\right) \Gamma'_X(\omega'; \theta'), \quad (8)$$

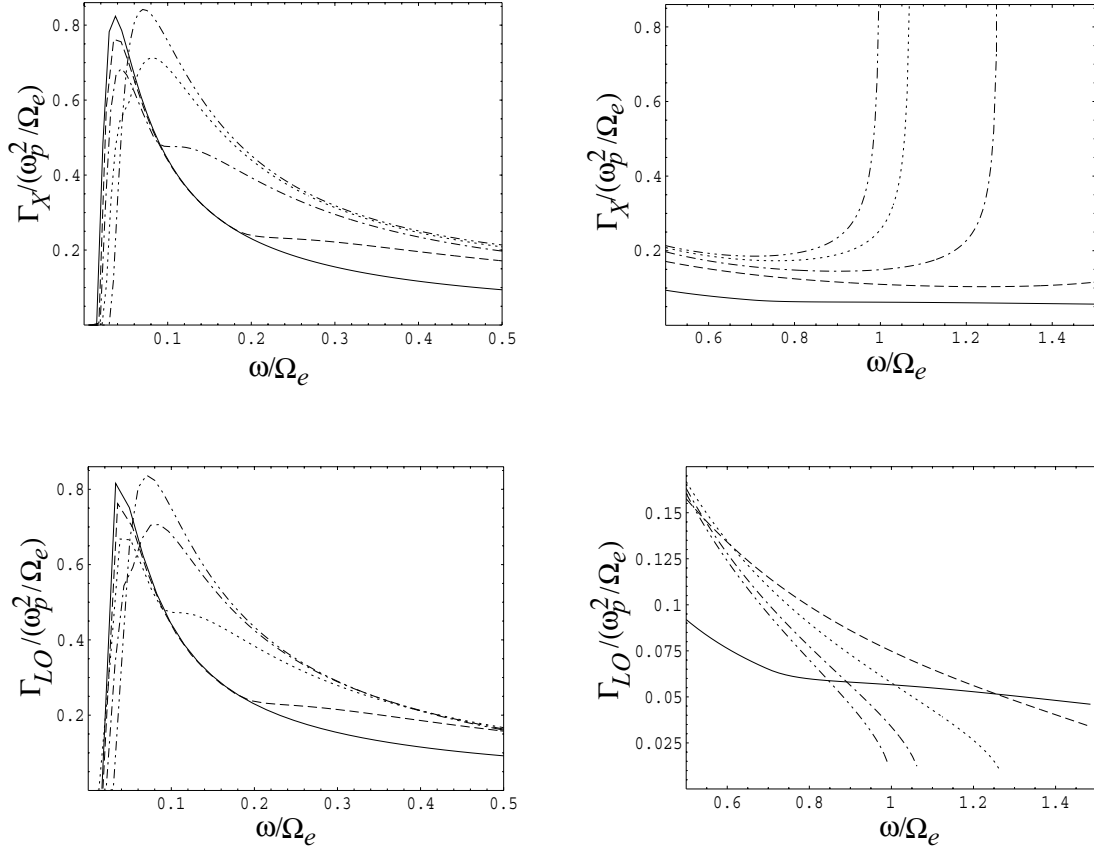


Figure 3. The cyclotron absorption coefficient, Γ_M , using the soft bell distribution in the plasma frame for the X and LO modes. The plasma parameters are $\langle\gamma\rangle = 10$ and $\omega_p/\Omega_e = 10^{-3}$ (corresponding to $v_a = 320$). The propagation angles are: $\theta = 0.1$ rad (solid); 0.6 (dotted); 0.9 (dot-dashed); 1.2 (dashed); and 1.5 (double dot-dashed).

where the primed quantities refer to the plasma rest frame and v_s is the bulk plasma velocity. Alternatively, one may transform the individual components on the right-hand side of Γ_M in (2) to the pulsar frame. The coefficient can be written approximately as

$$\begin{aligned} \Gamma_X(\omega; \theta) &\approx 160 \frac{M}{P} (1 - v_s \cos \theta) \\ &\approx 160 \frac{M}{P} \frac{\theta^2}{2} \quad \text{for } \gamma_s \gg 1 \text{ and } \theta \geq 0, \end{aligned} \quad (9)$$

with the condition

$$\frac{\omega}{\Omega_e} \sim \frac{1}{\langle\gamma'\rangle \gamma_s (1 - v_s \cos \theta)} \approx \frac{2}{\langle\gamma'\rangle \theta^2}, \quad (10)$$

and with $z \approx \sec \theta$ and $\omega_p^2/\Omega_e = 380M/P$. The relation $\omega_p^2/\Omega_e = 380M/P$ applies to secondaries with a multiplicity M relative to the Goldreich–Julian density, which is proportional to Ω_e/P , where P is the rotational period of the pulsar.

Relation (9) is the approximation of the absorption coefficient in the resonance region defined by relation (10). Recalling $\Omega_e \propto R^{-3}$, it follows from (10) that the radial distance of the resonance region, R_{res} , is

$$\begin{aligned} R_{\text{res}} &\approx \left[\frac{2\Omega_{e*}}{\omega \langle\gamma'\rangle \gamma_s \theta_{\text{res}}^2} \right]^{1/3} \\ &= 71.1 \frac{R_*}{\theta_{\text{res}}^{2/3}} \left(\frac{10^{10} \text{s}^{-1}}{\omega} \frac{10^2}{\langle\gamma'\rangle} \frac{10^2}{\gamma_s} \right)^{1/3} \\ &\quad \times \left(\frac{P \dot{P}}{10^{-15} \text{s}} \right)^{1/6}, \end{aligned} \quad (11)$$

where θ_{res} is the propagation angle in the resonance region, and R_* is the radius of the star. Our discussion assumes that R_{res} is inside the light cylinder, which corresponds to $R_{\text{res}}/R_* \lesssim 10^5(P/1\text{s})$.

As noted in Section 2.3, Γ'_M takes on different forms in four propagation angle bands, as a result of cyclotron absorption due to particles with velocities of either $v_{\parallel} = v_{r-}$ or $v_{\parallel} = v_{r+}$. The corresponding θ in the pulsar frame is found for $n \approx 1$ using

$$\cos \theta = \frac{\cos \theta' - v_s}{1 - \cos \theta' v_s}. \quad (12)$$

As θ increases from zero for $\gamma_s \gg 1$, θ' increases rapidly through oblique forward angles to backward angles (cf. Table 1). The first three bands, (i)–(iii) in Table 1, apply close to the dipole axis in the core region of the emission beam. The dependence $\Gamma_M \propto \theta^2$ implies that these are unimportant for cyclotron absorption. Significant absorption may be associated with band (iv), for which the resonance region is $\omega'/\Omega_e \approx (0.2\text{--}2) \langle\gamma'\rangle$ in the plasma frame. The

Table 1. The four propagation angle bands in the plasma and pulsar frames.

Band	Source	θ' (rad)	θ (rad)
(i)	v_{r-}	0.00–1.10	0.00–0.60/ γ_s
(ii)	v_{r+}	1.10–1.57	0.60/ γ_s –1.00/ γ_s
(iii)	v_{r-}	1.57–2.04	1.00/ γ_s –1.60/ γ_s
(iv)	v_{r+}	2.04–3.14	1.60/ γ_s –3.14

corresponding radial width of the resonance region, ΔR_{res} , in the pulsar frame is

$$\Delta R_{\text{res}} \approx 1.2 R_{\text{res}}, \quad (13)$$

implying an absorption region.

2.5 Resonance region

In discussing cyclotron absorption we assume the rays to be straight lines in a non-rotating dipole field; the effect of rotation is discussed in detail in Section 3. Polar coordinates, (R, χ) , aligned with the magnetic dipole axis are used. Rays are described by their propagation angle as a function of radial distance, $\theta(R)$, in the form

$$\theta(R) \approx \frac{3}{2}[\chi_0 - \chi(R)], \quad (14)$$

$$\chi(R) = \cos^{-1} \left[\frac{R_0}{R} \cos(\chi_0 + \psi_0) \right] - \psi_0, \quad (15)$$

$$\tan \psi_0 = \frac{3 \cos^2 \chi_0 - 1}{3 \cos \chi_0 \sin \chi_0}, \quad (16)$$

where $(R, \chi) = (R_0, \chi_0)$ and $\theta(R_0) = 0$ are the initial conditions, and $\tan \psi_0$ is the tangent to the field line at (R_0, χ_0) . The absorption regions for rays originating from three different radial distances are shown in Fig. 4. These are overlaid with the contour plots of the resonance radius $R_{\text{res}}(\omega, \theta)$.

2.6 Optical depth

The optical depth, τ , for absorption, corresponding to a damping factor $e^{-\tau}$ for the wave energy, is given by integrating either the spatial absorption coefficient with respect to distance, or the temporal absorption coefficient with respect to time, along the ray path. The latter gives

$$\tau = \int \Gamma_M dt. \quad (17)$$

For $\tau \ll 1$ cyclotron absorption has no significant effect, and for $\tau \gg 1$ no radiation escapes, so that practical interest is for $\tau \sim 1$.

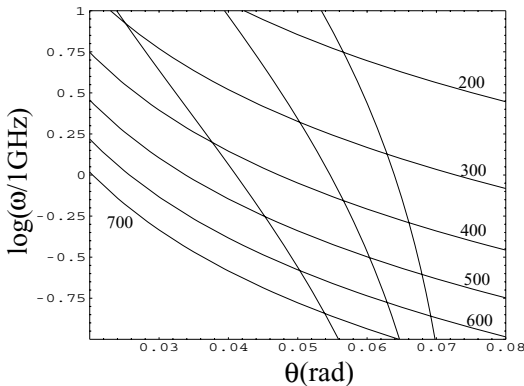


Figure 4. Resonance region. The three steep sloping lines correspond to the rays starting at $R_0 = 50, 100$ and 200 (from right to left), with $\chi_0 = 0.1$. The contours labelled with numbers are the resonance condition for $R_{\text{res}} = 200$ to 700 , defined by (10). We assume $\langle \gamma \rangle \approx \gamma_s = 200$ and $(P, \dot{P}) = (1, 10^{-15})$.

Using results from Section 4.1, a relevant approximation to τ for cyclotron absorption is

$$\begin{aligned} \tau &\approx \Gamma_M \Delta R_{\text{res}} / c \\ &\approx 0.5 \left(\frac{M}{10^3} \right) \left(\frac{10^3}{\langle \gamma \rangle} \frac{10^3}{\gamma_s} \right)^{1/3} \left(\frac{P \dot{P}}{10^{-15} \text{ s}} \right)^{1/6} \\ &\quad \times \left(\frac{10^{10} \text{ s}^{-1}}{\omega} \right)^{1/3} \left(\frac{\theta_{\text{res}}}{0.1} \right)^{1/3} \left(\frac{P}{1 \text{ s}} \right)^{-2/3}, \end{aligned} \quad (18)$$

where the numerical values are chosen to illustrate the dependence on plasma, pulsar and wave parameters for $\tau \sim 1$. Marginal absorption places a significant constraint on the plasma parameters, which is plausibly satisfied near the limits suggested by recent calculations of the cascade process, e.g. $M \sim 10^2$ and $\gamma_s, \langle \gamma \rangle \sim 10^2$ (Hibschman & Arons 2001).

Absorption is insensitive to \dot{P} , varying only as $\dot{P}^{1/6}$, but is sensitive to P , being stronger for faster pulsars. Recalling that θ_{res} is generally higher in faster pulsars, the requirement that τ not be so large as to allow radiation to escape places a severe constraint on plasma parameters in fast young pulsars. The dependence of τ on θ also implies higher absorption for the outer components of the emission beam than for the inner components. The absorption is stronger at lower frequencies, varying as $\tau \propto \omega^{-1/3}$.

The foregoing results are consistent with those of previous authors (Blandford & Scharlemann 1976; Lyubarskii & Petrova 1998). For example, the frequency condition for absorption given by (10), in the angular band (iv), is consistent with equation (69) of Blandford & Scharlemann (1976). (Their condition was also used by LM.) The optical depth given by (10) is consistent with the one in the cold plasma approximation (Lyubarskii & Petrova 1998).

3 ABSORPTION ACROSS THE EMISSION BEAM

3.1 Ray tracing in a rotating medium

Absorption across the emission beam is calculated numerically including the rotation of the medium. Since the cyclotron resonance is encountered far from the stellar surface, to a first approximation it is reasonable to assume that refraction has no effect on the wave modes. The condition for refraction not to affect the LO mode at $\omega \gg \omega_c$ corresponds to $v'_a \gg 1$ (the Alfvén speed in the plasma rest frame) in the resonance region, which is shown in Section 2 to hold in most magnetospheres. The modes can be treated as vacuum-like modes, propagating in straight lines in the inertial *observer* frame. Damping occurs in the open field line region within the LC, where the plasma corotates with the magnetic field. In the non-inertial *corotating* frame, the field is assumed to be dipolar. The Γ_M can be evaluated in the observer frame by making Lorentz transformations to the *local inertial* frame that corotates with the star.

Waves are assumed to be generated in one of the natural modes and beamed initially parallel to \mathbf{B} in the corotating frame. Consider two coordinate frames with the 3-axis along $\boldsymbol{\mu}$ and $\boldsymbol{\Omega}$, respectively. Their rotational transformations are shown in Fig. 5. The pulsar rotates with angular velocity $\boldsymbol{\Omega}$, with the dipole axis $\boldsymbol{\mu}$ inclined at an angle α to $\boldsymbol{\Omega}$. The two frames are assumed to have their (1, 3)-planes parallel to each other at one instant, subject to a clockwise rotational transformation $T_2(\alpha)$ by α about the 2-axis, which aligns $\boldsymbol{\Omega}$ with $\boldsymbol{\mu}$. The two frames corotate with the star, and after a time interval t , a clockwise rotational transformation, $T_3(\boldsymbol{\Omega} t)$, by $\boldsymbol{\Omega} t$,

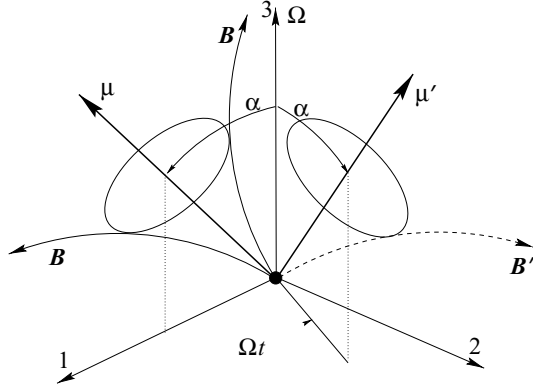


Figure 5. The geometry of a rotating pulsar magnetosphere is shown to illustrate the rotational transformations between the frames. The polar axis of the observer frame is along μ and that of the corotating frame along μ' .

about the 3-axis brings the (1, 3)-plane to align with the (Ω, μ') plane. The combined rotation is described by

$$T_{\mu}^{\mu'} = T_2(\alpha)T_3(\Omega t)T_2(\alpha)^{-1}. \quad (19)$$

This is followed by a Lorentz boost to the *local corotating* frame

$$L_{\mu}^{\mu'} = L(v)v_{\mu}^{\mu'}, \quad (20)$$

determined by the local corotation velocity $v = \Omega \times R$ (cf. Fig. 5). In this frame, Γ_M is evaluated as in Section 2.

In ray tracing, a Lorentz transformation is first made to the inertial observer frame and ray paths are calculated as a function of time, t , in this frame, using a coordinate frame with the 3-axis along μ at emission. Along a path, the local inertial corotating frame is found using a sequence of transformations.

The emission at a given frequency is assumed to originate at a single height, denoted by its radius $R_0 \sim 10\text{--}100R_*$, within the open field line region. At the emission radius, the emission beam is assumed to be generated with a two-dimensional (2D) distribution for its intensity. The beam is represented by a bundle of rays that reflects the 2D distribution for its intensity, and the shape of this distribution is assumed to be unchanged as the rays are refracted. Hence, the emission profile seen by the distant observer is described by the initial 2D distribution for its intensity centred on the final wavevector, k_f , of the central ray. The optical depth across the beam is reconstructed from τ for all rays. The pulse profile for a particular line of sight is then represented by a constant co-latitude cut through the beam in spherical polar coordinates aligned with ω , and the pulse phase is represented by the azimuthal angle.

The model for the plasma density has both a simple radial dependence and a cross-field or transverse dependence. The transverse dependence is assumed to be (e.g. Barnard & Arons 1986)

$$N = N_* \frac{1}{R^3} \exp \left[-\epsilon \left(\frac{\chi - \chi_c R^{1/2}}{\chi_c R^{1/2}} \right)^2 \right], \quad (21)$$

where χ is the polar angle relative to the pole, N_* is the surface density and χ_c denotes the ‘critical field line’ on which the density is a maximum. The factor ϵ indicates the transverse gradient in the plasma density, with $\epsilon = \epsilon_1$ for $\chi < \chi_c$, and $\epsilon = \epsilon_2$ for $\chi > \chi_c$. It is reasonable to assume that χ_c approaches that of the last open field line, $\chi_c \sim \chi_m$, and that $\epsilon_1 < \epsilon_2$.

We assume that in the corotating frame the geometry is a dipole, originating from a circular polar cap. Estimates of more accurate field geometry and corotation velocity involve details of the

electrodynamics of the magnetosphere that are not considered here. Specifically, we neglect currents that cause field line distortions and lower the corotation velocity (Michel 1991). These neglected effects become increasingly significant as the LC is approached.

3.2 Optical depth across emission beams

The 2D profile for cyclotron absorption is shown in Fig. 6, evaluated exactly for several illustrative sets of parameters. Parameters in each set are chosen so as to give marginal absorption. Profiles exhibit the basic dependence on parameters as discussed in Section 2. With the same propagation angle and plasma condition, there is no significant difference between absorption for the X mode and the LO mode, shown in Figs 6(a) and (b). However, the two modes can be absorbed very differently if they are emitted in the region well below the resonance region. In this case refraction can result in different propagation angles when the two reach the resonance region. The remaining profiles are determined only for the X mode. Absorption is axisymmetric to μ in an aligned rotator, increasing away from the axis due to field line curvature, and leaving a central underdamped spot. The spot drifts to the trailing edge of the cone as α increases, shown in Fig. 6(c). For a more relativistic plasma, Fig. 6(d), absorption is low, and the spot is narrow and towards the beam centre, with absorption increasing rapidly near the spot, and then gradually further away. When R_0 is closer to the surface, the spot is closer to the trailing edge of the beam. This also occurs for faster pulsars. Absorption across the beam may change if the plasma density depends on angle, Fig. 7(a).

One of the most distinctive features is the preferential absorption of the leading components of the beam. This is shown in Fig. 8 for an orthogonal rotator. This result is different from the one obtained by assuming a dipole in the observer’s frame, in which the trailing component tends to be preferentially absorbed (e.g. LM). If we assume a dipole in the corotating frame, at R_{res} the rays that form the leading component have larger propagation angle (cf. Appendix B) and are subject to stronger absorption than the ones forming the trailing component. This implies that the leading component is more absorbed than the trailing component. This result is valid in the absence of a transverse density gradient. When the density gradient is included, a stronger absorption of the trailing component can be seen at a certain viewing angle, as shown in Fig. 7(b).

4 APPLICATION TO PULSARS

The strength of cyclotron absorption in individual pulsars is determined principally by the parameters $\langle \gamma \rangle$ and M ; it increases with decreasing $\langle \gamma \rangle$ and increasing M . At a fixed frequency, the location of the cyclotron absorption region depends on the strength of the surface magnetic field, B_* , and on $\langle \gamma \rangle$; it moves away from the star with increasing B_* and with decreasing $\langle \gamma \rangle$. The location of the absorption region moves away from the star as the frequency decreases. The discussion here assumes that the absorption region is inside the light cylinder, and this requires that the absorption occur at a radius $R_{\text{res}}/R_* \lesssim 10^5(P/1s)$. With R_{res} given by (11), this condition is plausibly satisfied for a broad class of pulsars provided that the Lorentz factors are as low as recent calculations of the pair cascade process suggest (Zhang & Harding 2000; Hibschan & Arons 2001).

Our detailed calculations are directed at identifying observational signatures of marginal cyclotron absorption, $\tau \sim 1$. Our estimate for τ , cf. (18), suggests that for the relatively low Lorentz factors now

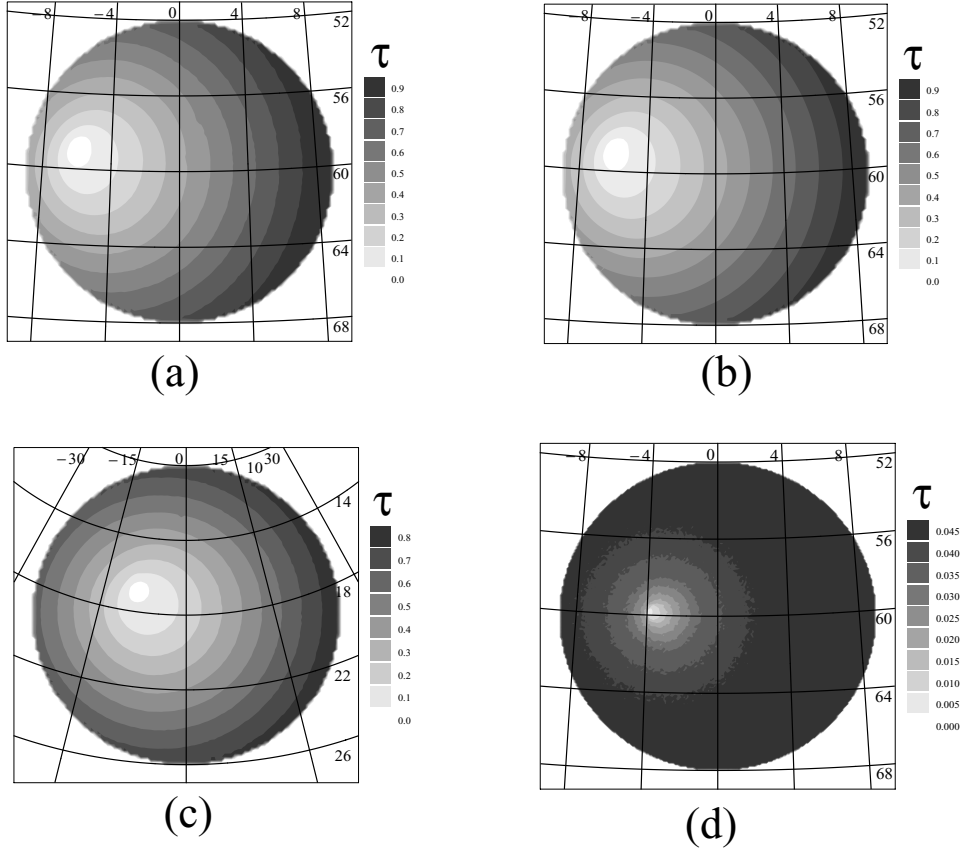


Figure 6. The optical depth for cyclotron absorption, τ , across the emission beam. The grid of longitudinal and latitudinal coordinates represents the azimuthal and polar angles (degree) of the rotational axis, with positive longitude corresponding to the leading half of the beam. Each part has a set of model parameters $(\alpha, \langle \gamma \rangle, R_0)$, where the rays are emitted at the radius R_0 (in R_*), as follows: (a) $(\pi/3, 10^2, 10^2)$ (X mode); (b) $(\pi/3, 10^2, 10^2)$ (LO mode); (c) $(\pi/10, 10^2, 10^2)$ (X mode); and (d) $(\pi/3, 10^3, 10^2)$ (X mode). We assume $\omega = 10^{10} \text{ s}^{-1}$, $(P, \dot{P}) = (1\text{s}, 10^{-15})$, $\gamma_s = \langle \gamma \rangle$, and $M = 10^2$ for all.

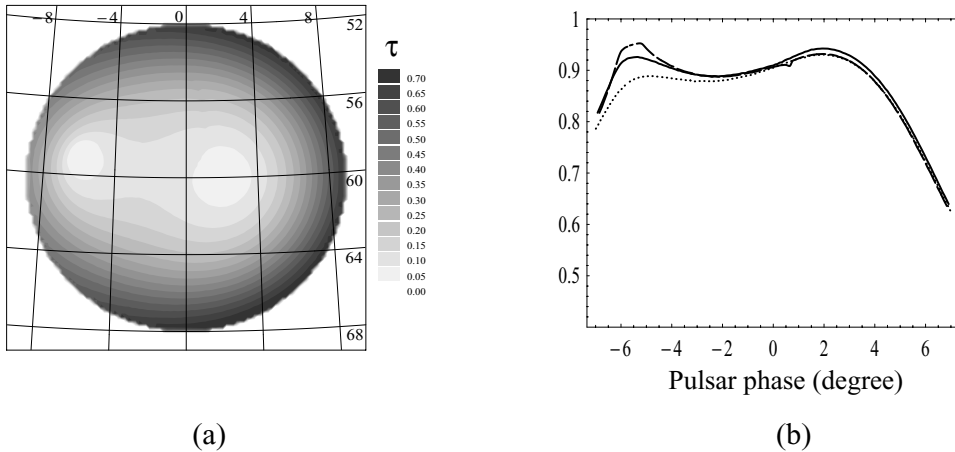


Figure 7. Pulse asymmetry due to cyclotron absorption. (a) The optical depth for cyclotron absorption across the emission beam as in Fig. 6(a) but with transverse gradient in plasma density with $\epsilon_1 = 3$, $\epsilon_2 = 4$ and $\chi = 0.8\chi_m$. (b) The intensity (in relative scale) versus pulsar phase for the viewing angles, 59° (solid), 60° (dashed) and 61° (dotted). The initial intensity at the emission radius is assumed to be uniform across the open field line flux tube.

favoured in polar-cap models (Zhang & Harding 2000; Hibschan & Arons 2001), cyclotron absorption should be strong enough to have observable consequences for a broad class of pulsars. Indeed, these estimates suggest that cyclotron absorption within the LC may even be relevant to the entire pulsar population, including millisecond pulsars.

The numerical evaluation of absorption across the emission beam suggests possible observational signatures for absorption. The radio beam becomes axially asymmetric as a result of cyclotron absorption coupled with corotation. Since $\tau \propto M\theta^2$, both the asymmetry in θ and the density gradient can cause the radio beam to have axially asymmetric absorption. When the asymmetry in θ is dominant in

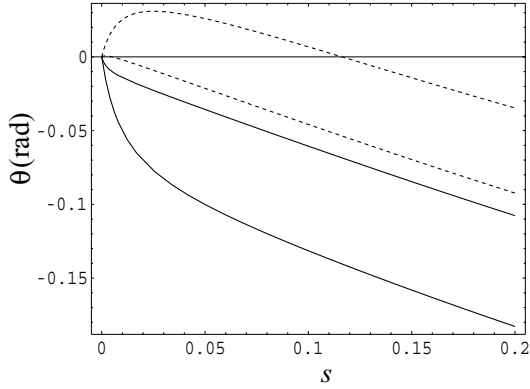


Figure 8. Asymmetric propagation angles in an orthogonal rotator. Trajectories in leading components are solid and those for trailing components are dashed. The outer pair correspond to the ray originating from ($R = 0.01 R_{LC}$, $\theta = \pm 0.1$) on the last open field lines. The inner pair represent the propagation angle for the ray originating from ($R = 0.0025 R_{LC}$, $\theta = \pm 0.01$) on the open field line with a smaller latitude, $\theta_*/\theta_d = 0.25$, where θ_d is the half opening angle of the polar cap.

determining the absorption, there is a preferential damping in the leading component of the pulse profile. If the asymmetric absorption is predominantly due to the transverse plasma density gradient, the trailing component can be preferentially absorbed. As shown in Fig. 7, asymmetry in the pulse profile depends on the viewing angle. In Fig. 7(b), a stronger leading component can be seen at the viewing angle 59° or 61° . Observations appear to suggest that there are relatively more pulsars with leading components with a higher intensity (Blaskiewicz et al. 1991). Lyne & Manchester (1988) classified conal double-component pulse profiles, where both components are from the cone or outer beam, and they found that the leading component is dominant for 53 pulsars compared to 24 for which the trailing component is dominant. This suggests that the transverse plasma density gradient may play a significant role in producing asymmetric absorption.

There is little difference between absorption for the X mode and the LO mode across the emission beam. However, this may not be the case in models in which refraction of the LO mode is important. (Refraction has little effect on the X mode.) For simplicity we assume that the two modes propagate in the same direction when entering the resonance region; however, if refraction causes the two modes to have substantially different propagation angle, then they may experience substantially different rates of cyclotron absorption.

Another important characteristic of cyclotron absorption is its sensitivity to frequency. In the weak or marginal absorption regime ($\tau < 1$), cyclotron absorption modifies spectra by a factor, $\propto \omega^{-1/3}$, which is a relatively weak function of frequency. However, if the absorption is strong, $\tau > 1$, it may cause a low-frequency cut-off in the spectrum. More generally, any signatures of cyclotron absorption across the emission beam should be stronger at lower frequencies.

In our discussion we concentrate on marginal absorption, $\tau \sim 1$, but the estimates suggest that absorption could be strong, $\tau \gg 1$, for a fraction of all pulsars. However, cyclotron absorption must not be strong along all prospective escape paths, at least in observed pulsars. In order for any radiation to be observed, one requires that there be at least some ray paths along which absorption is at most marginal. If the signatures of such marginal absorption are identified in observational data, they will give significant insight into the pulsar radio emission process.

5 SUMMARY

We consider cyclotron absorption in relativistic pulsar plasmas including the effect of plasma corotation with the star. We assume that the radio emission is produced in either the X mode or the LO mode in an emission region, and that this radiation passes through a cyclotron absorption region along its escape path. Absorption across the radio beam is evaluated numerically, and it is shown that significant asymmetry arises from the effect of rotation and of density gradient in the pair plasma distribution. Such asymmetry in the pulse profile should be observable. To make ray-tracing calculation more efficient, we assume a relatively large emission radius so that refraction of the rays is not important. Our results should not be strongly dependent on this neglect of refraction, but it does preclude discussion of differential absorption of the X and LO modes, due to only the latter experiencing significant refraction.

Our results are relevant for marginal absorption. However, plausible estimates suggest that absorption may be strong in a broad class of pulsars. This raises an important dilemma concerning how any radiation escapes if cyclotron absorption is indeed as strong as these estimates suggest. This dilemma was apparent from earlier discussions of cyclotron absorption (Blandford & Scharlemann 1976; Mikhailovskii et al. 1982), and it is not clear how it is to be resolved. Nevertheless, radiation does escape at least from those pulsars that are observed, and these estimates make it plausible that cyclotron absorption may have observable effects on the escaping radiation.

ACKNOWLEDGMENT

We thank Michael Gedalin for useful discussion.

REFERENCES

- Arendt P. N., Jr, Eilek J. A., 2002, *ApJ*, 581, 451
- Arons J., 1983, *ApJ*, 266, 215
- Arons J., Barnard J. J., 1986, *ApJ*, 302, 120
- Asseo E., Khechinashvili D., 2002, *MNRAS*, 334, 743
- Barnard J. J., Arons J., 1986, *ApJ*, 302, 138
- Blandford R. D., Scharlemann E. T., 1976, *MNRAS*, 174, 59
- Blaskiewicz M., Cordes J. M., Wasserman I., 1991, *ApJ*, 370, 643
- Daugherty J. K., Harding A. K., 1982, *ApJ*, 252, 337
- Gedalin M., Melrose D. B., Gruman E., 1998, *Phys. Rev. E*, 57, 3399
- Hibschman J. A., Arons J., 2001, *ApJ*, 560, 871
- Kazebegi A. Z., Machabeli G. Z., Melikidze G. I., 1991, *MNRAS*, 253, 377
- Kennett M. P., Melrose D. B., Luo Q., 2000, *J. Plasma Phys.*, 64, 333
- Luo Q., Melrose D. B., 2001, *MNRAS*, 325, 187 (LM)
- Lyne A., Manchester R. N., 1988, *MNRAS*, 234, 477
- Lyubarskii Yu. E., Petrova S. A., 1998, *A&A*, 337, 433
- Melrose D. B., Gedalin M. E., 1999, *ApJ*, 521, 351
- Melrose D. B., McPhedron R. C., 1991, *Electromagnetic Processes in Dispersive Media*. Cambridge Univ. Press, Cambridge
- Melrose D. B., Gedalin M. E., Kennett M. P., Fletcher C. S., 1999, *J. Plasma Phys.*, 62, 233
- Michel F. C., 1991, *Theory of Neutron Star Magnetospheres*. Univ. Chicago Press, Chicago
- Mikhailovskii A. B., Onishechenko O. G., Suramlishvili G. I., Sharapov S. E., 1982, *Sov. Astron. Lett.*, 8, 369
- Ruderman M. A., Sutherland P. G., 1975, *ApJ*, 196, 51
- Shibata S., Miyazaki J., Takahara F., 1998, *MNRAS*, 295, L53
- Sturrock P. A., 1971, *ApJ*, 164, 529
- Weise J. I., Melrose D. B., 2001, *MNRAS*, 329, 115
- Zhang B., Harding A. K., 2000, *ApJ*, 532, 1150

APPENDIX A: CYCLOTRON ABSORPTION COEFFICIENTS
A1 Dielectric tensor

For a non-gyrotropic pulsar plasma, the dielectric tensor can be written as (e.g. Melrose & Gedalin 1999; Melrose et al. 1999; Kennett et al. 2000)

$$\begin{aligned}
 K_{11} &= K_{22} \\
 &= 1 - \frac{\omega_p^2}{\omega^2} \int_{-\infty}^{\infty} du_{\parallel} F(u_{\parallel}) \frac{\omega - k_{\parallel} v_{\parallel}}{\gamma} \left(\frac{1}{D_+} + \frac{1}{D_-} \right), \\
 K_{13} &= -\frac{\omega_p^2 k_{\perp}}{\omega^2} \int_{-\infty}^{\infty} du_{\parallel} F(u_{\parallel}) \frac{v_{\parallel}}{\gamma} \left(\frac{1}{D_+} + \frac{1}{D_-} \right), \\
 K_{33} &= 1 + \frac{2\omega_p^2}{\omega} \int_{-\infty}^{\infty} du_{\parallel} \frac{\partial F(u_{\parallel})}{\partial u_{\parallel}} \frac{v_{\parallel}}{\omega - k_{\parallel} v_{\parallel}} \\
 &\quad + \frac{\omega_p^2 k_{\perp}^2}{\omega^2 \omega_e} \int_{-\infty}^{\infty} du_{\parallel} F(u_{\parallel}) v_{\parallel}^2 \left(\frac{1}{D_+} - \frac{1}{D_-} \right), \tag{A1}
 \end{aligned}$$

where $D_{\pm} = \omega - k_{\parallel} v_{\parallel} \pm \Omega_e/\gamma$. The cyclotron resonance condition can be written as

$$\begin{aligned}
 D_+ D_- &= (\omega - k_{\parallel} v_{\parallel})^2 - \frac{\Omega_e^2}{\gamma^2}, \\
 &= k_{\parallel}^2 (1 + y^2) (v_{\parallel} - v_{r+})(v_{\parallel} - v_{r-}), \tag{A2}
 \end{aligned}$$

$$v_{r\pm} = \frac{\omega k_{\parallel} \pm \Omega_e (k_{\parallel}^2 - \omega^2 + \Omega_e^2)^{1/2}}{k_{\parallel}^2 + \Omega_e^2}. \tag{A3}$$

There are three relevant parameter regimes: the subluminal region, $v_{\phi} < 1$, and two superluminal regions, $1 < v_{\phi} < [1 + (\Omega_e/k_{\parallel})^2]^{1/2}$ and $v_{\phi} > [1 + (\Omega_e/k_{\parallel})^2]^{1/2}$. The NCR can occur in either the subluminal region or the superluminal region $v_{\phi} < [1 + (\Omega_e/k_{\parallel})^2]^{1/2}$. The ACR can only occur in the subluminal region. There is no cyclotron resonance in the second superluminal region $v_{\phi} > [1 + (\Omega_e/k_{\parallel})^2]^{1/2}$.

A2 Absorption coefficients

The Landau prescription implies

$$\frac{1}{D_{\pm} + i0} = P \left(\frac{1}{D_{\pm}} \right) - i\pi \delta(D_{\pm}), \tag{A4}$$

and one obtains

$$\begin{aligned}
 K_{11}^A &= K_{22}^A \\
 &= i\pi \frac{\omega_p^2}{\omega^2} \int_{-1}^1 dv_{\parallel} \gamma^2 F(\gamma v_{\parallel}) (\omega - k_{\parallel} v_{\parallel}) \\
 &\quad \times [\delta(D_+) + \delta(D_-)], \tag{A5}
 \end{aligned}$$

$$K_{13}^A = i\pi \frac{\omega_p^2 k_{\perp}}{\omega^2} \int_{-1}^1 dv_{\parallel} \gamma^2 v_{\parallel} F(\gamma v_{\parallel}) [\delta(D_+) + \delta(D_-)],$$

$$\begin{aligned}
 K_{33}^A &= -i\pi \frac{2\omega_p^2}{\omega} \int_{-1}^1 dv_{\parallel} \gamma^3 v_{\parallel} \frac{\partial F(u_{\parallel})}{\partial u_{\parallel}} \delta(\omega - k_{\parallel} v_{\parallel}) \\
 &\quad - i\pi \frac{\omega_p^2 k_{\perp}^2}{\omega^2 \omega_e} \int_{-1}^1 dv_{\parallel} \gamma^3 v_{\parallel}^2 F(\gamma v_{\parallel}) [\delta(D_+) - \delta(D_-)].
 \end{aligned}$$

APPENDIX B: PROPAGATION ANGLE IN THE COROTATION FRAME

To derive the propagation angle in the corotation frame, we assume that the magnetic field is a static dipole in this frame. The tangent to a curved ray is

$$\tan \psi_{\text{ray}} \approx \frac{\sin(\psi - s) - r \sin(\chi + s)}{\cos(\psi - s) + r \cos(\chi + s)}, \tag{B1}$$

where $r = R/R_{\text{LC}} \ll 1$, and ψ is the tangential angle at the origin ($s = 0$) of the ray. In the pulsar frame, the ray follows a straight line. The tangent to a dipole field line is given by

$$\tan \psi_f = \frac{3 \cos^2 \chi - 1}{3 \sin \chi \cos \chi}. \tag{B2}$$

The angle ψ is determined from (B1) and (B2). Assuming $\tan \psi_f = \tan \psi_{\text{ray}}$ at $s = 0$, we have

$$\sin(\psi - \psi_0) = r_0 \sin(\psi_0 + \chi_0), \tag{B3}$$

where $r_0 = r(s = 0)$, $\psi_0 = \psi_f(s = 0)$ and $\chi_0 = \chi(s = 0)$. Then, the propagation angle, $\theta = \psi_{\text{ray}} - \psi_f$, is given by

$$\tan \theta = \frac{\tan \psi_{\text{ray}} - \tan \psi_f}{1 + \tan \psi_{\text{ray}} \tan \psi_f}. \tag{B4}$$

This paper has been typeset from a $\text{\TeX}/\text{\LaTeX}$ file prepared by the author.